Single-compartment model of a pyramidal neuron, fitted to recordings with current and conductance injection

Anton Chizhov, Dmitry Amakhin, A. Erdem Sagtekin, Mathieu Desroches

Single-compartment model of a pyramidal neuron, fitted to recordings with current and conductance injection

Anton V. Chizhov[1,2*], Dmitry V. Amakhin[3], A. Erdem Sagtekin[4,5], Mathieu Desroches[1]

1 MathNeuro Team, Inria Centre at Universite Cote d'Azur, Sophia Antipolis, France

2 Computational Physics Laboratory, Ioffe Institute, Saint Petersburg, Russia

3 Laboratory of Molecular Mechanisms of Neural Interactions, Sechenov Institute of Evolutionary Physiology and Biochemistry of the Russian Academy of Sciences, Saint Petersburg, Russia

4 Istanbul Technical University, Istanbul, Turkey

5 University of Tuebingen, Tuebingen, Germany

***** anton.chizhov@inria.fr

Abstract

For single neuron models, reproducing characteristics of neuronal activity such as the firing rate, amplitude of spikes, threshold potentials etc. as functions of both synaptic current and conductance is a challenging task. In the present work, we measure these characteristics of regular spiking cortical neurons using the dynamic patch-clamp technique, compare the data with predictions from the standard Hodgkin-Huxley and Izhikevich models, and propose a relatively simple five-dimensional dynamical system model, based on threshold criteria. The model contains a single sodium channel with slow inactivation, fast activation and moderate deactivation, as well as, two fast repolarizing and slow shunting potassium channels. The model quantitatively reproduces characteristics of steady-state activity that are typical for a cortical pyramidal neuron, namely: firing rate not exceeding 30 Hz; critical values of the stimulating current and conductance which induce the depolarization block not exceeding 80 mV and 3, respectively (both values are scaled by the resting input conductance); extremum of hyperpolarization close to the midpoint between spikes. The analysis of the model reveals that the spiking regime appears through a saddle-node-on-invariant-circle (SNIC) bifurcation, and the depolarization block is reached through a saddle-node bifurcation of cycles. The model can be used for realistic network

simulations, and it can also be implemented within the so-called mean-field, refractory density framework.

Keywords: pyramidal neuron, dynamic patch-clamp, shunting effect, Hodgkn-Huxley approximation, dynamic threshold

Statements and Declarations

The authors have no competing interests.

1. Introduction

Relatively simple models of single neurons that are quantitatively fitted to experiments are helpful for biophysically detailed large-scale simulations and also to derive mean-field limits. Many such models have been developed, but to date none of them reproduce all features of neuronal activity. Specifically, to the best of our knowledge, there is no model that reproduces the following 4 characteristics of neuronal steady-state firing of the principal neurons of the cerebral cortex. First, a typical pyramidal cortical neuron shows maximum firing rate in a range from 20 to 50 Hz (Fernandez et al. 2011; Bianchi et al. 2012). Second, the depolarization block (DB) appears at a critical value of the injected current values from 40 to 100 mV, if scaled by the resting input conductance (Bianchi et al. 2012; Smirnova et al. 2015). Third, there is a critical value of the synaptic conductance that shunts spiking activity for any injected current; it is typically on the order of 1 to 10 times the value of the resting-state input conductance. And fourth, in a typical spike train, the time elapsed since the last spike until the moment when the membrane potential reaches its minimum, is typically between 10 and 30 ms.

In contrast to those facts, even complex multicompartmental models tend to overestimate the firing rate and the size of the domain of steady-state firing in the 2D space of synaptic current and conductance. They also tend to produce a more abrupt rapid transition towards the minimum of membrane voltage following a spike than it is observed in experiments with pyramidal cortical neurons. Moreover, in most studies proposing neuronal models, important aspects such as the depolarization block, the shunting effect of synaptic conductance and/or the voltage trace shape, are ignored or not considered together.

We strongly emphasize the significance of these characteristics. Our first condition is essential because the maximum firing rate is the most important characteristic of a neuron as a pulse generator. Many of the existing models based on the Hodgkin-Huxley formalism predict much higher maximal firing rates and critical values of injected current inducing the depolarization block. Because of this reason, the f-I curves are usually plotted only for the limited range of currents. Such overestimation of firing rate might lead to inadequate simulations of neuronal network phenomena. For instance, overestimated firing rates might result in altered relationship between

neuronal firing and dynamics of ionic concentrations, which is crucial for the development of epilepsy models (Cressman et al. 2009; Krishnan and Bazhenov 2011; Wei et al. 2014; Chizhov et al. 2019). As shown, the transition of neurons into depolarization block plays a crucial role in some regimes of epileptic activity (Krishnan and Bazhenov 2011; Wei et al. 2014), however models used in those works are based on single neuron models that are too “strong” in the sense of maximum firing rates and the range of input currents and conductances. This quantitative discrepancy leads to a biased tuning of ionic dynamics parameters for reproduction of network activity patterns, thus making the comparison with experiments rather qualitatively but not quantitatively correct.

Most simplified models of neuronal firing aim to reproduce the realistic firing pattern in response to a current injection at a fixed level of membrane conductance, but not at different values of conductance within physiological range. However, under physiological conditions, neurons fire in response to the activation of synaptic conductances, and moreover, the synaptic activation cannot provide pure current-clamp conditions. The importance of shunting effect is shown, for instance, in studies of visual cortex, in experiments (Borg-Graham et al. 2003) and simulations (Chizhov and Graham 2021). In contrast, the fitting of neuronal models to experiments and their comparison are typically done with datasets obtained from only current-clamp recordings (Gerstner and Naud 2009). Our second and third criteria require the fitting and comparison to a set of data that include various input conductances. The criteria characterize the domain of steady-state spiking in the 2d space of the main control signals received by the neuron, namely, the synaptic current and conductance (Pokrovskii 1978; Shriki et al. 2003). These signals determine the first two, voltage-independent and linearly voltage-dependent components of the total input current received by a neuron from synaptic populations (Pokrovskii 1978). The input conductance might be modulated with the help of the dynamic clamp technique (Destexhe and Bal 2009; Graham and Schramm 2009) or optogenetics (Berndt et al. 2014). These techniques have not been used specifically for the purpose of neuron model construction. Instead, a canonical technique was based on the voltage-clamp and current-clamp recordings (Hodgkin and Huxley 1952). Whereas this technique is able, in principle, to reveal full information about the dynamics of each of pharmacologically isolated voltage-dependent channels, it does not allow to probe a pharmacologically intact neuron as a complex dynamical system in the full range of its input (synaptic) signals. Such probing requires a separate consideration, similar to the one proposed in the present work.

The fourth one, the voltage minimum, is an important aspect of the voltage evolution between spikes that features the composition of underlying ionic currents, determines the state of inactivation of sodium channels and, consequently, the probability and amplitude of the next spike (Shao et al. 1999; Vervaeke et al. 2006).

The mentioned four features are in the focus of the present work. We build a model that belongs to the class of minimal single-compartment conductance-based models realistically reproducing voltage traces and shape of spikes, like those considered in the study by Pospischil et al. (Pospischil et al. 2008). In addition, our model is targeted to reproduce the four aforementioned characteristics, as well as to maintain biophysical details at the level of distinction of different gating variables for the most effective ionic channels. In contrast to more simplified models like the Izhikevich model (Izhikevich 2003), the adaptive exponential integrate-and-fire (AdEx) (Brette and Gerstner 2005) or the conductance-based adaptive exponential integrate-and-fire (CAdEx) (Gorski et al. 2020), able to simulate different types of neurons with their different patterns of spiking activity corresponding to different settings of intrinsic parameters, our model mimics just an individual real neuron which, however, is typical within the class of regular spiking cortical neurons in the rat's brain. Therefore, our work does not contain any analysis on variation of intrinsic parameters, but instead studies neuronal dynamics as a function of input signals. For illustrative purposes, we compare our experimental data and model with one of the simplified models.We propose a dynamic threshold model. In terms of single-compartment modeling of a neuron, the approximation of spike activation with a dynamic threshold lies behind the conceptual framework of the independence of activation and inactivation within the Hodgkin-Huxley formalism. An example of a model with inter-dependent activation and inactivation gating variables can be found in (Naundorf et al. 2006), where the proposed one-compartment model captures two observations that are contradictory in the frameworks of the standard Hodgkin-Huxley one-compartment description. These observations are the large variability of somatically registered spike thresholds and the sharp kinks of voltage at spike initiation. It is known (Gutkin & Ermentrout 2006; McCormick et al. 2007) that these effects are explained by spatial dynamics of action potential initiated at the axonal initial segment. However, within the framework of a single-compartment description, the former model from (Naundorf et al. 2006) is still a useful phenomenological model. In (Chizhov et al. 2014), we considered an additional experimental observation, the so-called divisive effect of rate-versus-current gain decrease with additional shunt. These three observations together have been reproduced using a 3-state Markov model, in which the activation threshold was dependent on the slow inactivation. The present work is more focused on quantitative comparison of the four characteristics mentioned above with data.

We present experimental data obtained from principal, presumably pyramidal neurons of rat cortex using the whole-cell patch-clamp method. The data illustrate the variability of the above-mentioned characteristics of neuronal activity. Within the recorded cells, we choose a single representative one and fit the model to this particular cell. We propose a hybrid model of moderate complexity (5 ordinary differential equations (ODEs)) which satisfies the above-mentioned criteria. It includes a dynamic threshold-based approximation for one type of sodium channels and Hodgkin-Huxley-type approximations for fast and slow potassium channels. The model reveals a

few elements that are crucial for consistency with the experiments: the medium-scale inactivation of sodium channels, the prolonged high-conductance state between spikes, the slow inactivation of potassium channels and the dependence of the activation threshold on slow inactivation for sodium channels.

The proposed model distinguishes three types of voltage-dependent channels and reveals their role in spike generation, which is a prediction that is testable in experiments with pharmacological blockade of distinct fast and slow potassium channels. The model also highlights the interdependence of sodium channel activation on inactivation. Note, that these gating characteristics are the ones observable with somatic recordings, and are, in this sense, effective gating variables. That interdependence and the threshold dynamics are also testable predictions. However, even considering the proposed model as just a mechanistic description of spike generation that captures its important characteristics, it is useful for the development of neuronal population models that can be further employed to simulate realistic large-scale network simulations, for instance with the help of the refractory density approach (Schwalger and Chizhov 2019).

The rest of the article is organized as follows. In Section 2, we present experimental results on pyramidal neurons' firing activity and characteristics, which are challenging for existing models. In Section 3, we highlight the limitations of existing models in reproducing key characteristics from these data, and we introduce our model, showing that it matches the experiments according to all four above-mentioned criteria. In Section 4, we summarize our findings and propose a few perspectives. Finally, the experimental and computational methods are reviewed in the Appendix.

2. Experimental results

2.1 The firing rate of a representative cortical neuron is a function of stimulating current and conductance

With the help of the dynamic-clamp technique (Prinz et al. 2004; Destexhe and Bal, 2009), we injected into neurons the voltage-dependent current $I_{inj}(U,t) = u(t) - s(t)(U(t) + 60mV)$, setting the steps of current $u(t)$ and conductance $s(t)$ with a duration of 1500ms. Notice that the assignment of the two signals $u(t)$ and $s(t)$ is equivalent to the assignment of an arbitrary set of synaptic conductances $g_s(t)$ and reversal potentials V_s, assuming the conductances to be independent of the membrane potential $U(t)$ (Smirnova et al. 2015). This is the reason why $u(t)$ and $s(t)$ are expressed via the voltage-independent synaptic conductances: $s(t) = \sum_s g_s(t)$ and $u(t) = \sum_s g_s(t)(V_s + 60mV)$, where the chosen reversal potential, -60mV, is an arbitrary fixed constant. In order to characterize the steady-state firing regime, we calculated for each pair of values (u,s) the firing rate $f(u,s)$ as the number of spikes per time unit starting at 1/3 of the

stimulus duration. As seen from Fig.1A plotted for a representative pyramidal cortical neuron, the domain of nonzero stationary firing rate is limited; on the left, the inclined boundary corresponds to subthreshold currents and on the right, the almost vertical boundary does to currents leading to the depolarization block. As seen from several representative traces with the same firing rate (Fig1A, insets), corresponding to the points inside the excitation domain and lying on the same isoline, the spike shape, the dynamics of the spike amplitudes, and the minimum voltage depend on the conductance $s(t)$. At the same time, the timing of voltage reaching its minimum does not significantly depend on the shunting conductance $s(t)$.

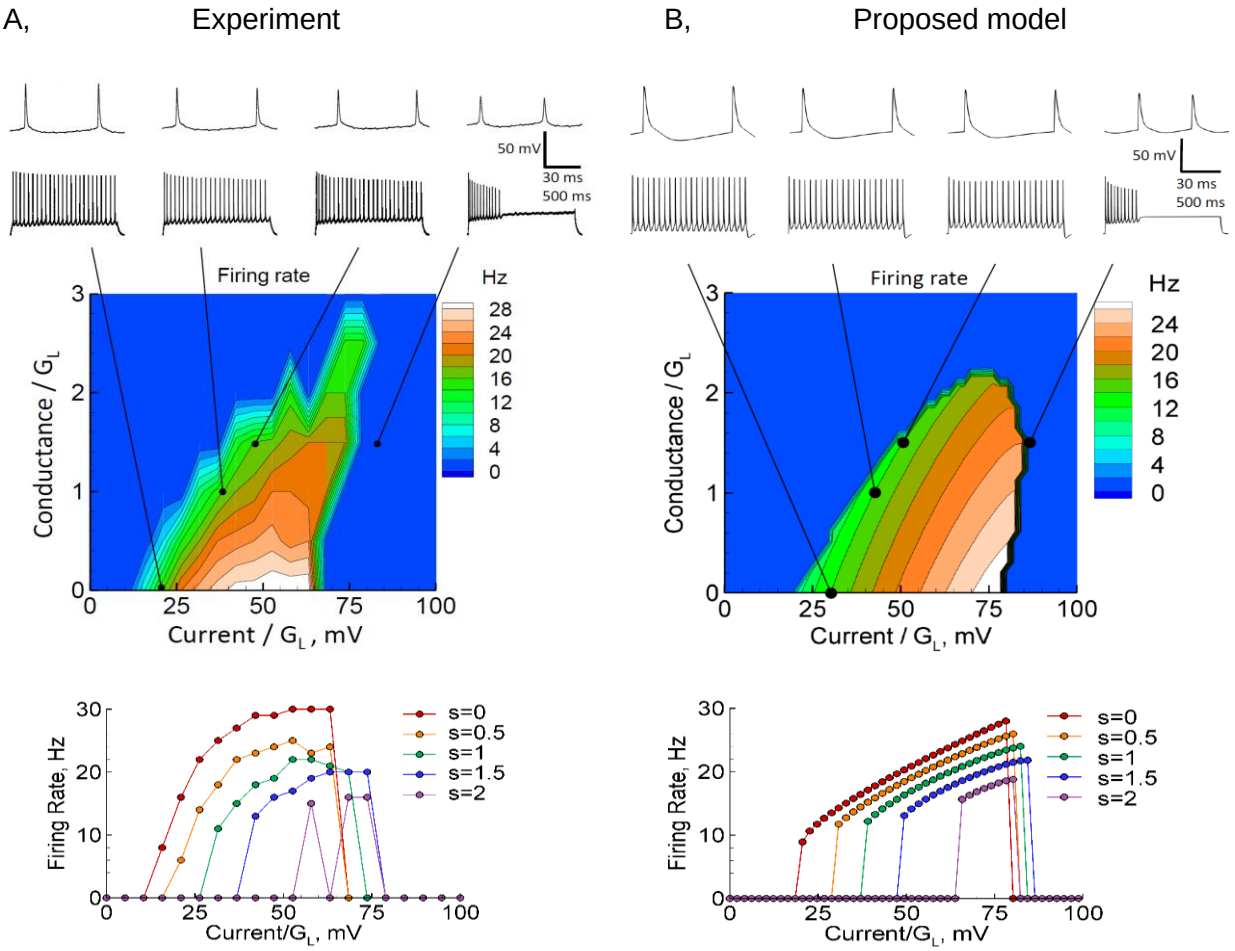

Figure 1. Experimental (A) and simulated (B) plots for the steady-state firing rate as a function of input current and conductance. The f-I curves at the bottom of each panel is an alternative representation of the same data. A, the data from pyramidal neuron of the medial frontal cortex of the rat brain. B, the model proposed in the present paper. In the bottom plots, the values of the conductance s are given in the units of the input conductance G_L.

The f-u-s plot (Fig.1A) is in focus of the present study; it is used as a benchmark for comparison between different mathematical models (Fig.1B, Fig.2).

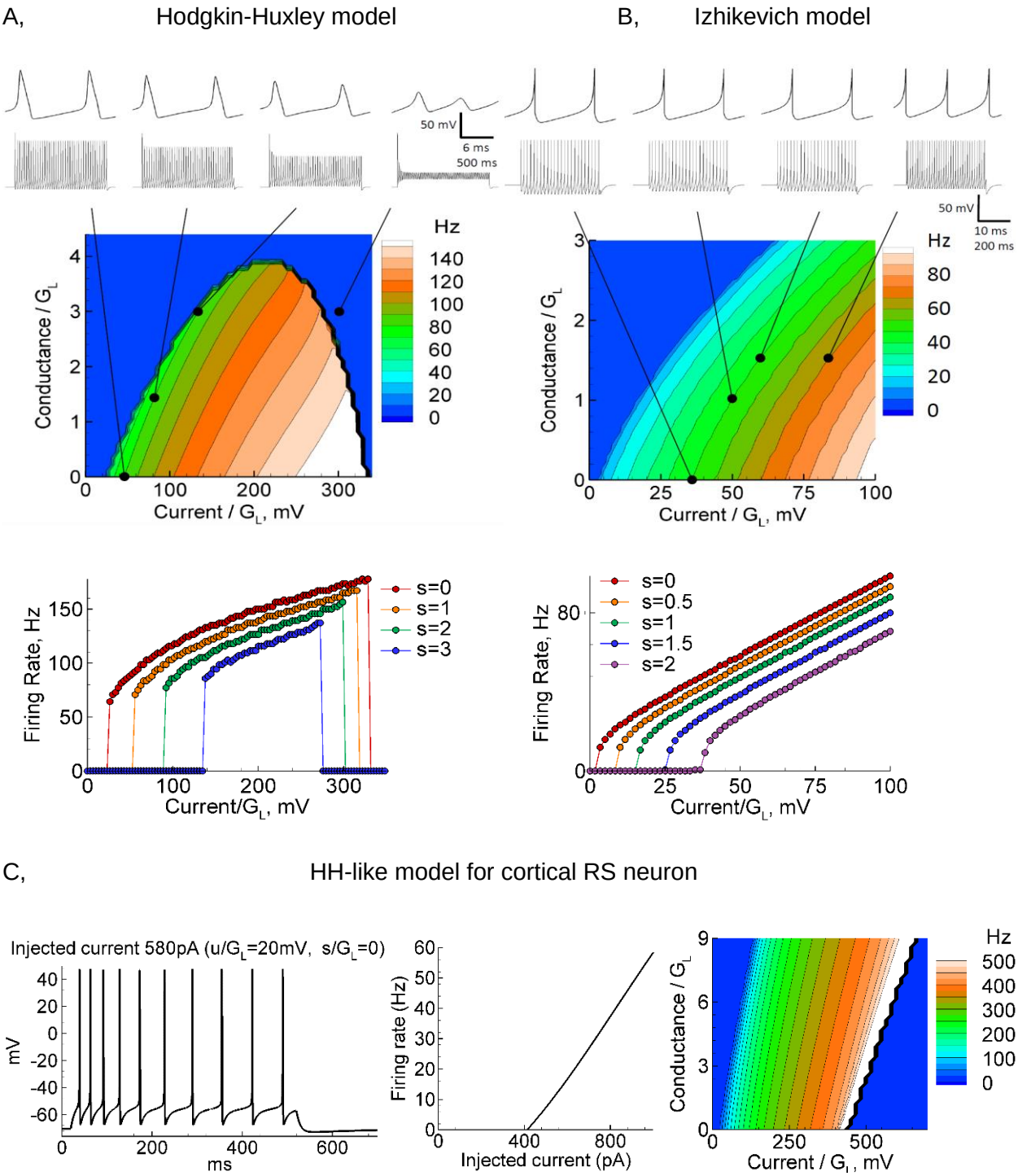

Figure 2. Simulated plots for the steady-state firing rate as a function of input current and conductance. A, the standard Hodgkin-Huxley model. B, the Izhikevich model for regular spiking neuron. C, the Hodgkin-Huxley-like minimal model for cortical regular spiking (RS) neuron (Pospischil et al. 2008).

2.2 Real neurons have dispersed characteristics

The obtained plots for the firing rate $f(u,s)$ are shown in Fig.3 for several pyramidal neurons of the prefrontal cortex, which were recorded in similar experimental conditions. The plots have similar “tongue”-like shapes and represent a tendency for the firing rate to increase with the stimulating current u and to decrease with the stimulating conductance s. The variability of the plots reflects the individual characteristics of the neurons. The observed range for the DB critical current u/G_L is from 40 to 150 mV; the range for the maximum of s/G_L is from 0 to 6 (for a number of cells n=10); the maximum firing rate varies from 18 to 32 Hz. As the variability of these firing characteristics is high, we decided to not average them, but to focus on a single representative neuron instead.

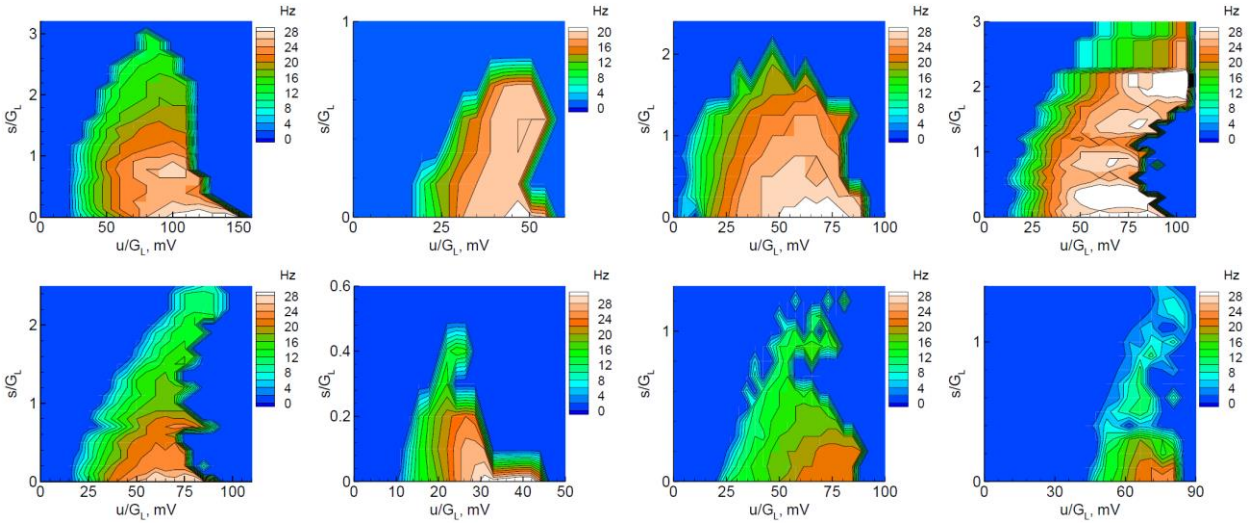

Figure 3. Experimentally measured firing rate versus current and conductance for 8 neurons.

2.3 The characteristics of spike shapes and voltage evolution are functions of both stimulating current and conductance

Not only the firing rate but also the other characteristics of stationary firing, including the shape of spikes and the voltage evolution between the spikes, depend on the two stimulation parameters, u and s. As seen from Fig.4A (top row, middle), the somatically observed voltage threshold of a spike initiation, V^T, is varied in a range of at least 10mV. It reaches the highest values at the brink of DB, so the approach to DB is reflected in the increase of V^T.

The average voltage between spikes (see the Appendix) (Fig.4A, top row, right) increases by about 15mV for the 60 mV increase of u/G_L. Dividing these two values, we estimate the conductance averaged across time and all traces, and thus obtain $4G_L$. This conductance is 4 times bigger than the membrane conductance at rest, G_L, because of the contribution of voltage-gated channels that remain to be opened on interspike intervals. Moreover, these channels dominate over the passive leak, meaning that the real neuron can hardly be represented by a leaky integrate-and-fire model. Because of the shunting provided by the slow voltage-gated

channels, the average depolarization is much smaller than the one predicted by a passive leak model based on the input conductance G_L. For instance, the average voltage deflection from the resting value (-65mV) at $u/G_L = 50mV$ and $s = 0$ is about 25mV, which is twice as less as u/G_L. These observations indicate that the persistent or slow changing shunting affects the neuronal membrane potential.

The peak voltage at spikes (Fig.4A, bottom row, left) is maximal at the threshold current and minimal at the DB boundary, dropping by about 20mV. The spikes widen with the current (Fig.4A, bottom row, middle), doubling the half-amplitude width at the DB boundary in comparison to the spikes at the threshold current. The minimum between spikes, which we call the post-spike hyperpolarizing potential (V_{PHP}), varies in a range of about 14mV, increasing towards the DB boundary (Fig.4A, bottom row, right). The voltage difference $V^T - V_{PHP}$ decreases with the stimulating current or with V_{PHP}. Presumably, the decrease of $V^T - V_{PHP}$ results in DB.

A, experiment

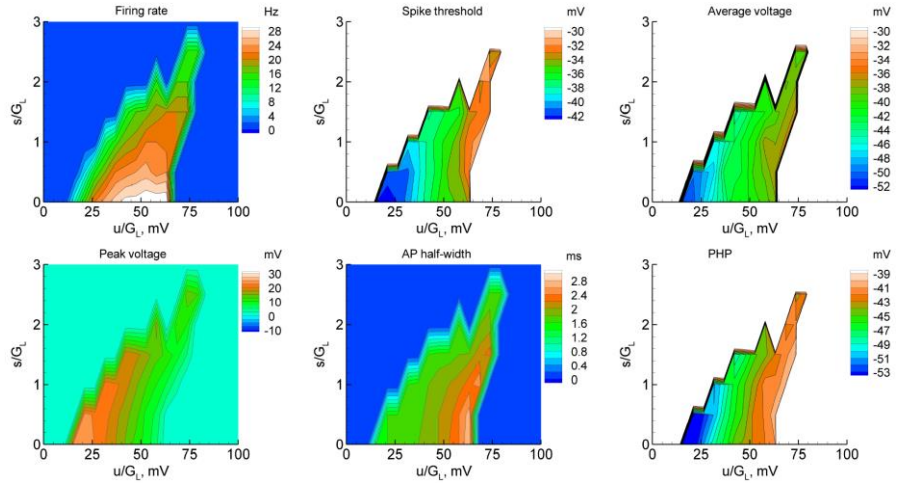

B, Hodgkin-Huxley model

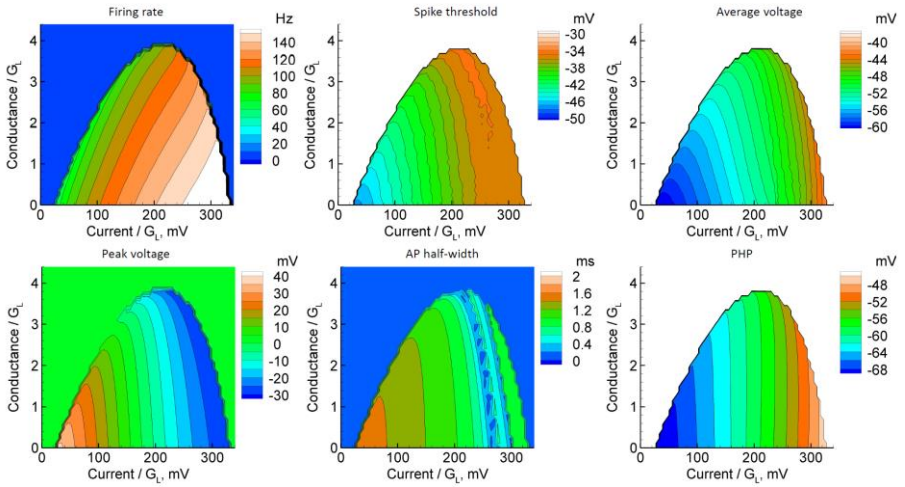

C, proposed model

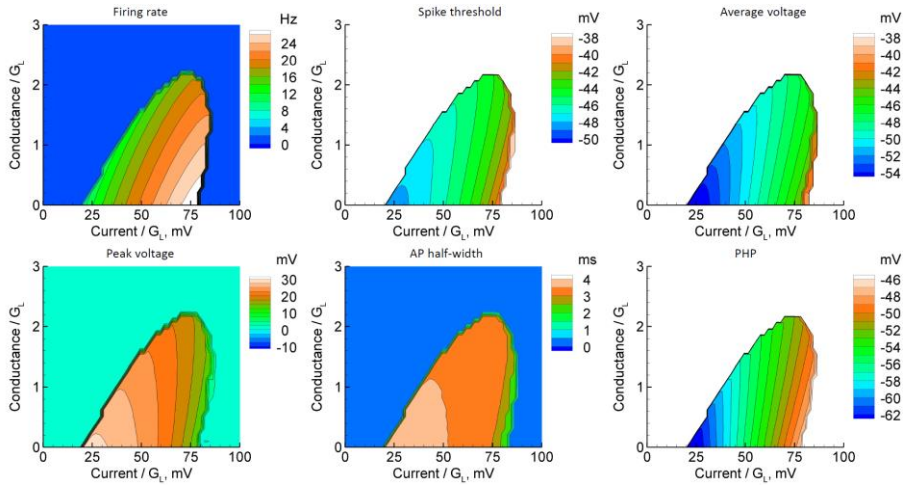

Figure 4. Experimentally measured and simulated neuronal characteristics versus current and conductance: firing rate, spike threshold, average voltage, peak voltage, half-width of action potential (AP)

and post-spike hyperpolarization potential (PHP). Left top panels in A and C for the firing rate are the same as in Fig.1.

3. Models

3.1 Canonical Hodgkin-Huxley model versus experiments

We ran the same protocols as in experiments with the standard one-compartment Hodgkin-Huxley model (Appendix A.2.1), based on the following equation for membrane potential

$$\frac{dU}{dt} = -g_L(U - V_L) - \overline{g}_{Na}\, m^3\, h\, (U - V_{Na}) - \overline{g}_K\, n^4 (U - V_K) + I_{inj}(U, t)$$

The details of the model and the notations are given in Appendix A.2.1.The only modification of the original model was the resting potential set to be -65mV. The input conductance at the resting potential was fitted to 5nS by setting the membrane area to be equal to $1.4 \cdot 10^{-5} cm^2$.

The standard Hodgkin-Huxley model correctly reproduces the experiments in many aspects, but with some notable disagreements (Fig.2A and 4B), namely:

(i) the shape of the domain of stationary firing is “tongue”-shaped (Fig.2A and Fig.4B, top left);

(ii) the firing rate increases with the stimulating current;

(iii) the maximum stimulating conductance is $4G_L$ (Fig.2A and 4B), which is in the experimental range (Fig.3);

(iv) the variability range of the spike threshold V^T (see the definition in the Methods section) was about 13mV (Fig.4B, top middle), which is as large as in experiments. However, the voltage evolution at the spike initiation is too smooth, which is because of the smooth sodium activation dependence. In the Hodgkin-Huxley approximation framework, it is impossible to sharpen the spike initiation without a decrease of the threshold variability range.

(v) the average voltage (see Appendix) range (about 18mV) (Fig.4B, top right) is consistent with the experiment, but the average conductance derived from this value and the underlying current u/G_L range (300mV) is about $16G_L$, which is 4 times bigger than in real neurons. So, the HH model overestimates the contribution of voltage-gated channels.

(vi) the peak voltage range (Fig.4B, bottom left) is large, between -30 and 30mV.

(vii) the spike width at the half-height (see Appendix) (Fig.4B, bottom middle) does decreases, which contradicts the experimental observatons.

(viii) the minimal voltage V_{PHP} (Fig.4B, bottom right) decreases with the current in a consistent range of about 25mV. This range is larger than for V^T, which means that $V^T - V_{PHP}$ is decreasing, as in the experiment.

(ix) the time elapsed since last spike until reaching the minimum of the membrane potential crucially differs from that in the experiment (3 versus 20ms; compare Fig.5B to 5A).

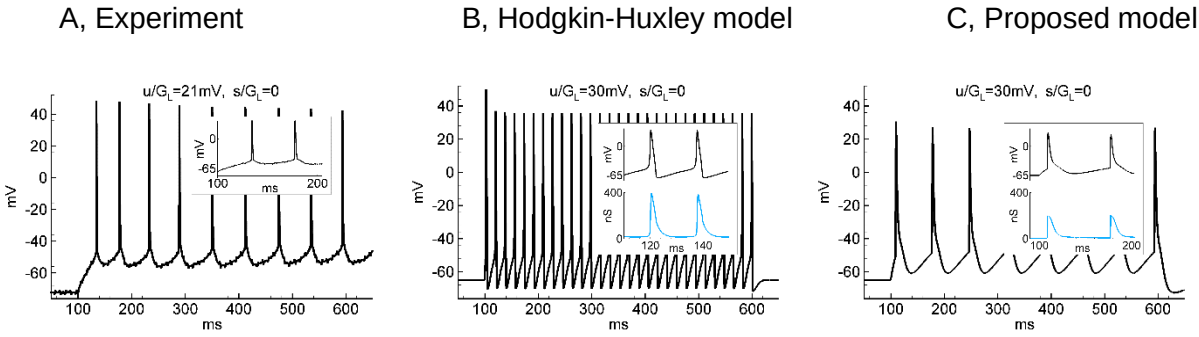

Figure 5. Experimentally measured and simulated spike trains. The timing of voltage minima in the Hodgkin-Huxley model significantly differs from those in the experiment and in the proposed model (insets) because of an overestimation of the total membrane conductance (blue).

Summarizing our observations, we conclude that the HH model reproduces qualitatively well the steady-state characteristics of firing of our representative neuron, but the quantitative comparison is not satisfactory. Presumably, the main crucial discrepancy is the overestimation of the shunting provided by voltage-gated channels.

3.2 Minimal Hodgkin-Huxley-like model for regular spiking neuron

A reader may suppose that the above mentioned discrepancies between the standard Hodgkin-Huxley model and our experimental data might be due to the difference in registered neurons. The original model has been developed for a giant squid axon, whereas our data are for cortical regular spiking neurons. To verify this aspect, we have considered a minimal Hodgkin-Huxley-like model (Appendix A.2.2) fitted to experimental data obtained in cortical regular spiking neurons of rodents (Pospischil et al. 2008):

$$\frac{dU}{dt} = -g_L(U - V_L) - \overline{g}_{Na}\, m^3\, h\, (U - V_{Na}) - \overline{g}_K\, n^4 (U - V_K) - \overline{g}_M p (U - V_K) + I_{inj}(U, t),$$

where a slow potassium channel with the activalion variable $p(U, t)$ was added to the original Hodgkin-Huxley model.

The experimental data set was obtained in the current-clamp mode, so the fitting was performed for only an injected current as a stimulus, using voltage traces with spike trains and f-I curves. The examples of a simulated spike train and an f-I curve are presented in Fig.2C (left and middle).

However, the extended simulations with additional input conductance show atypical behaviour with a widening of excitation domain for large s (Fig.2C, right). This comparison underlies the importance of fitting models to data that probe shunting effects.

3.3 Izhikevich model versus experiments

The simple model proposed by Izhikevich (Izhikevich 2003) is the model of a different level of description, aimed to reproduce spiking patterns for different types of neurons depending on the intrinsic parameter settings. We use this model here for illustrative purposes, as a representative of the class of simplified, two-dimensional models. By construction, this family of models does not allow modeling of depolarization block. For a regular spiking cell (Appendix A.2.3), the model shows spikes that are similar to the real neuron's spikes (Fig.2B), in sense of their sharp shapes, amplitude and duration; and the firing rate depends on both of the input signals, u and s. On the other hand, contrary to the experiments, the model does not reproduce the depolarization block, overestimates the maximum firing rate (Fig.2B), underestimates the dependence of spike amplitude on u and s, and reaches the voltage minimum too early after each spike.

3.4 Our proposed model

We propose a model that consists of one sodium and two potassium channels with the Kirchhoff equation for the membrane potential $U(t)$ given as eq.(1) (see Appendix A2.4):

$$\frac{dU}{dt} = -g_L(U - V_L) - \overline{g}_{Na}\, m^2\big(U,t;h(U,t),V^T(i)\big)\; i(U,t)\,(U - V_{Na}) - \overline{g}_{K,f}\, n(U,t)(U - V_K) - \overline{g}_{K,s}\, w(U,t)(U - V_K) + I_{inj}(U,t)$$

The sodium channel approximation is of threshold-type, however it is written via the gating variables of non-dimensional conductance $m(U,t)$ and slow inactivation $i(U,t)$ (eq.(2)). At any time instant where the voltage $U(t)$ reaches the threshold $V^T(t)$, if the fast inactivation $h(U,t)$ is above 0.5, then the sodium channel is instantaneously activated (Fig.6A). This activation is described by instantaneous resetting of the variable $m(U,t)$ to 1 and $h(U,t)$ to 0, according to eq.(3), so activation implicitly depends on inactivation. The variables m and h then passively decay, according to eqs.(5,6). The variable m produces the typical time-course of the sodium conductance after a voltage-step activation (Fig.6C), which implicitly takes into account fast and moderate inactivation of the channels of pyramidal cells in adult animals (Hamill et al. 1991). The conductance depends not only on variable $m(U,t)$, but also on the slow inactivation $i(U,t)$, which is conventionally described in HH-like form, eq.(7). The threshold $V^T(t)$ also depends on the slow inactivation $i(U,t)$ according to eq.(4).

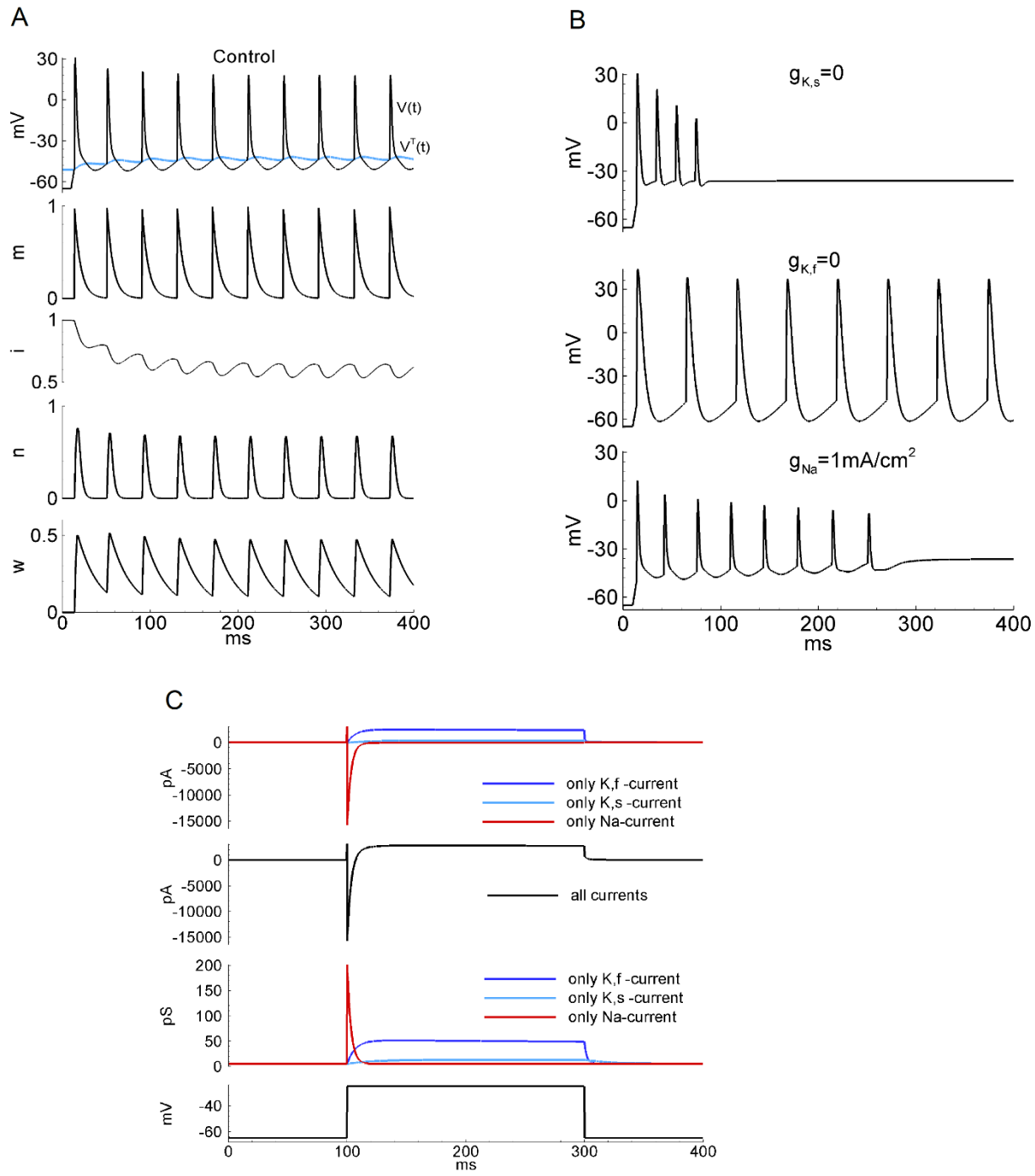

Figure 6. Simulated responses in current- and voltage-clamp modes. A,B, stimulation with 300pA current ($u/G_L = 60mV$). A, membrane potential, threshold potential (blue) and gating variables: sodium channel activation m, slow inactivation i, fast potassium activation n and slow potassium activation w. B, effects of the blockade of fast (top), or slow (middle) potassium currents, or the reduction of sodium current (bottom). C, voltage-clamp, currents and conductances as responses to a voltage-step.

Once activated at a spike, the sodium channels close on the time scale of milliseconds and thus terminate the spike even if potassium channels are blocked. However, fast potassium channels, activating at the initial phase of a spike, contribute to the repolarization and significantly shorten

the spike. We approximate this by one fast potassium channel, which is a conventional direct rectifier, eq.(8), with a single activation variable $n(U,t)$ evolving according to eq.(9). According to the approximation, the channel activates and deactivates at about $V_{1/2} = -25mV$, which approximately corresponds to the middle voltage level of a spike.

The slowly-evolving shunting is modelled with the slow potassium channel. It is approximated with one activation variable $w(U,t)$ according to eqs.(10,11). The channel activates at about the top of the spike $V_{1/2} = 0$, and it deactivates passively with the time scale $1/b = 20ms$. As a result, we have constructed a model based on 5 ODEs for the state variables U, m, i, n_f and n_s.

As seen from the comparison between simulations and the experimental data, the model reproduces most of the experimental observations (compare Fig.1B to 1A and Fig.4C to 4A):

1) the shape of the domain of stationary firing is “tongue”-shaped (Fig.4C, top left), and the DB boundary is almost vertical;

2) the firing rate increases up to the maximum rate about 28 Hz, as in the experiment;

3) the maximum current u at the DB boundary is about $80mV \cdot G_L$ (versus $70mV \cdot G_L$)

4) the maximum stimulating conductance s is 2.2 (versus 2.8);

5) the spike threshold V^T variability range (about 10mV) is as large as in the experiment;

6) due to threshold initiation of sodium channel the modelled spike has a sharp initiation and the discontinuous voltage increase rate with a distinguishable threshold, which is comparable to the experimental recordings;

7) the average voltage range is almost as large as in the experiment (12 versus 15mV);

8) the average voltage relative to the resting potential (-65mV) at, for instance, $u/G_L = 50mV$ and $s = 0$, is about 15mV, which leads to the average shunting $50mV \cdot G_L/15mV \approx 3.3G_L$, which is close to and does not exceed the experimentally estimated value of $4G_L$. Thus, the model does not overestimate the contribution of voltage gated channels.

9) the peak voltage is up to 25mV, and its range is about 15mV (versus 20mV).

10) the spike width is almost unchanged, in contrast to the experiment, however it at least does not decrease as in the HH model.

11) the minimal voltage V_{PHP} decreases with the current in the consistent range of about 14mV (versus 12 mV). The difference $V^T - V_{PHP}$ is decreasing, as in the experiment.

12) the time passed since spike until reaching the minimum by the membrane potential well corresponds to the experiment, with the voltage minimum being almost in the middle between the spikes (compare Fig.5C to 5A).

Among these observations, the items 2-4 and 12 justify that the proposed model satisfies the four conditions initially formulated in the Introduction.

3.4.1 Overestimation of membrane conductance in HH model

The above-mentioned estimates of the average conductance in the experiment and in the HH model have shown that the HH model overestimates the contribution of voltage-gated channels. Comparing the two models, we see that the proposed model generates a membrane conductance that is twice as small as the one generated by the HH model (Fig.5B,C).

3.4.2 Threshold dynamics and DB

The dynamic threshold dependence on slow inactivation, eq.(4), not only affects the firing rate as a function of input, but also determines the sequence of threshold values in a spike train. As seen from Fig.7A-D (green dots), this sequence is increasing in both experiment and model. The threshold variability is larger for strong stimuli; compare Fig.7A to 7B and Fig.7C to 7D. Because the slow inactivation $i(t)$ affects not only the threshold but also the sodium current, eq.(2), the thresholds reversely correlate with the peak membrane potential values (orange dots). The level of slow inactivation is approximately determined by the voltage minimum V_{PHP} (cyan dots), which is why the voltage difference between the minimum and the threshold, $V^T - V_{PHP}$, varies across spike trains, and within aspike train, less than the threshold V^T does across spike trains for different inputs. In this sense, V_{PHP} is a predictor of the threshold V^T at each following spike. For the case with strong stimulus, DB emerges after a gradual increase of V^T (Fig.7B,D) towards its steady-state, voltage-dependent values (Fig.7F), i.e., due to rising inactivation, that is, the decrease of $i(t)$ (Fig.7E, left blue). The inactivation $i(t)$ affects the firing properties by increasing the threshold and decreasing the peak values of the potassium channel activation variables, $n(t)$ and $n_A(t)$, which depend on the spike amplitude. In turn, the weakened potassium channels enhance the inactivation, i.e., decrease $i(t)$ from spike to spike. Therefore, the rising threshold is a cause of DB in the model.

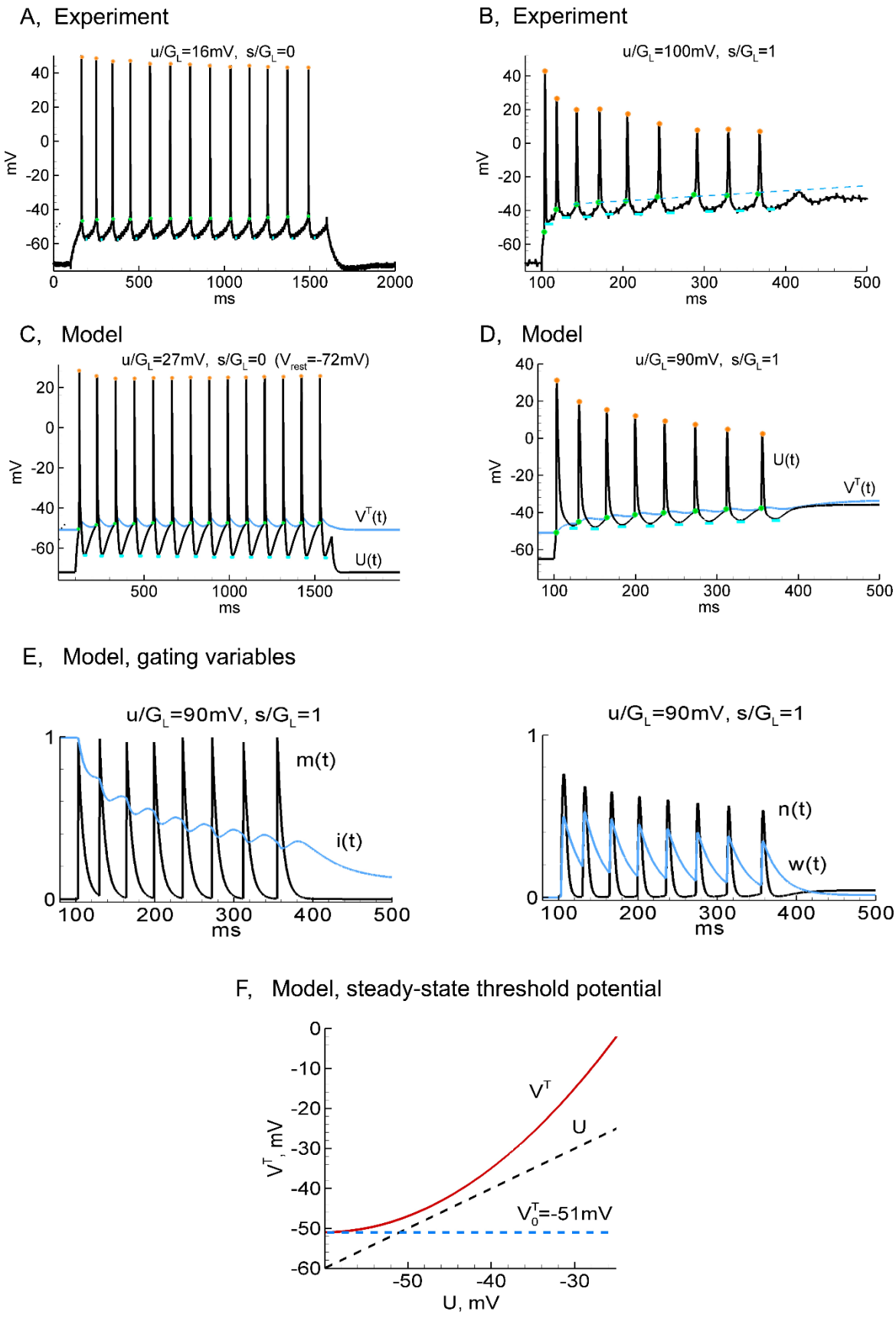

Figure 7. Experimental (A and B) and simulated (C -E) responses showing the dynamics of the spike threshold (green dots), the peak voltage (orange) and PHP (cyan) during the weak current stimulation (A and C) and during strong stimulus that leads to DB (B, D, and E). The blue solid line shows the modelled threshold, the blue dashed line is the linear fit for the threshold values at all spikes except the first two ones.

F, the steady-state voltage dependence of the threshold potential, $V^T(U) = -51 + ((U + 60)/5)^2\ mV$ (red), which is derived from eq.(4) after substitution $i = i_\infty$. The dashed straight lines shows the bisector (black) and the initial threshold level (blue).

3.5 The roles of the different channels included in the model

Each of the gating variables contributes to the spiking pattern. Their roles are revealed in simulations with the blockade of the channels (Fig.6B). The blockade of slow potassium channel leads to early DB (Fig.6B, top). In this case, the prolonged sodium current is no longer shunted between spikes, which leads to an accumulation of inactivation, an elevation of the threshold, and eventually DB. Thus, the slow potassium channel significantly affects the domain of spike generation. Another effect of this blockade is shortening the time since the last spike until the voltage minimum.

Blocking the fast potassium channel widens the spikes and decreases the firing rate (Fig.5B, middle). The decrease of sodium channel's maximum conductance results in the decrease of spike amplitudes, facilitates DB, and thus decreases the domain of spike generation (Fig.6B, bottom).

Overall, we conclude that the gating variables that we have introduced are important for the model to reproduce the four biophysical characteristics mentioned in the Introduction.

3.6 Bifurcation analysis

The scenario of initiation of the spike generation and the transition to DB can be explained with the help of bifurcation analysis (Fig.8), obtained for the continuous-time version of the proposed model, given in the Appendix A.2.5. Bifurcation diagrams characterize the asymptotic behavior of the model depending on given system's parameters that we choose to vary. They are represented with the main bifurcation parameter, the constant input u at zeroed s, on the horizontal axis, and the voltage variable on the vertical axis. We consider two different cases, namely, for intact threshold $V^T(t)$ (Fig.8A) and fixed threshold $V^T = -51\ mV$ (Fig.8B). In the transient case of time-dependent $u(t)$, the trajectory of the system may approach one of those two extreme cases. In the case of a response to a current step, the trajectory starts following the case of $V^T = -51\ mV$ (Fig.8B) and then gradually switches to the former case (Fig.8A). The bifurcation responsible for spike initiation corresponds to a saddle-node on invariant circle (SNIC) bifurcation, whereas the bifurcation responsible for the transition to DB corresponds to a saddle-node bifurcation of limit cycles (SNC) at large input values. Interestingly, the limit cycles in the case of intact $V^T(t)$ form an isola, whereby the fixed-point solution is stable in the entire range of u. Similar behavior has been found in, e.g., the simple model of a dopaminergic neuron (Dovzhenok and Kuznetsov, 2012). In our case, the isola exists because the steady-state voltage-dependent threshold is above the membrane potential itself in its entire range (the red line is above the dashed black bisector in

Fig.7F. Therefore, the dynamic threshold, eq.(4), determines the main features of the model's behavior.

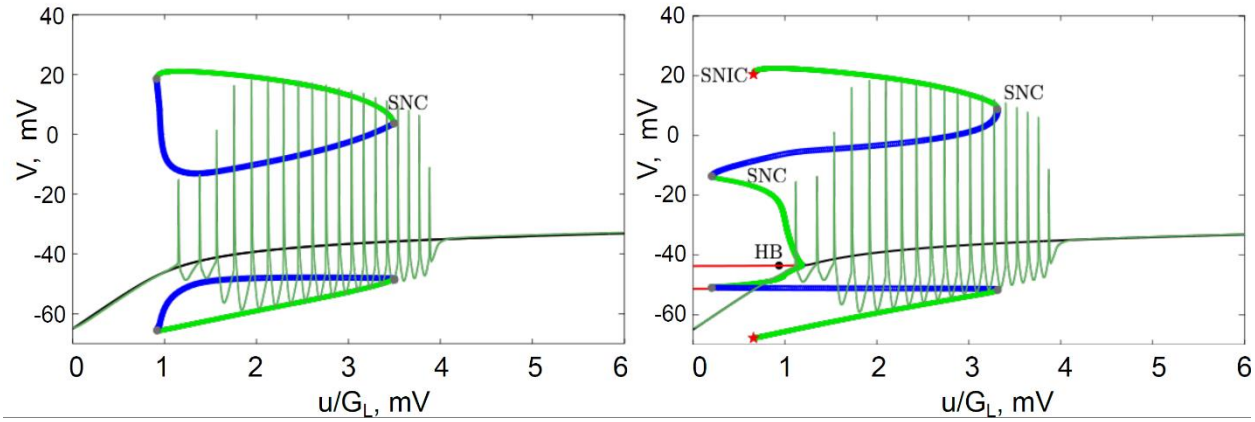

Figure 8. Bifurcation diagrams for the proposed model in the cases for the intact $V^T(t)$ (A) and the fixed threshold $V^T = -51\,mV$ (B). Bifurcations: SNC, saddle-node bifurcation of limit cycles; HB, Andronov-Hopf bifurcation; SNIC, saddle-node on invariant circle bifurcation. Black and red are stable and unstable fixed points, green and blue are stable and unstable limit cycles, respectfully. The dark green solution corresponds to the response to ramp shown in Fig.9C.

The presence of isola is reflected in the model's behavior in response to ramping stimuli for $u(t)$ (Fig.9). It is interesting that the response to "weak" ramp, where neuron does not reach DB (Fig.9B), shows more spikes than the response to "strong" ramp with DB (Fig.9C). The behavior is determined by the dynamics of the threshold, shown in blue in Fig.9, which in turn follows the slow inactivation variable. The DB is accompanied by strong inactivation that corresponds to a high level of the threshold, which is maintained during the ramp down (Fig.9C). On the bifurcation diagram (Fig.8B), the response to "strong" ramp is initially close to the fixed point solution (black line), then it turns into the large-amplitude oscillations and later, with some delay, close to the middle of the ramp, it returns to the fixed point. The delay effect is well known and due to the slow speed of the ramp; see e.g. (Rinzel & Baer, 1988). The quasi steady-state voltage level at this stage is always below the threshold, according to Fig.7F. Only fluctuations of voltage can transfer the system to spiking, which happens in presence of noise. Such spontaneous spike generation is seen in Fig.9D.

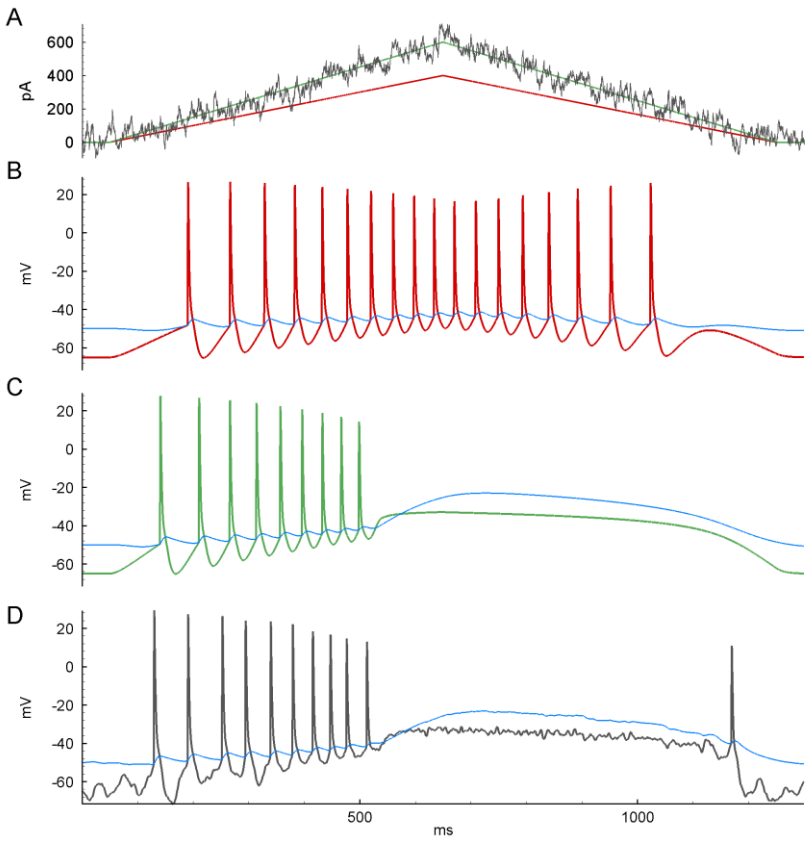

Figure 9. Responses to ramp stimuli (A) of the proposed model in the cases of relatively weak (up to 400pA) stimulus (B), strong (600pA) stimulus (C), and in presence of noise (D). The current-noise was realized as the Ornstein-Uhlenbeck process with the time constant 5ms and the amplitude 50pA.

4. Discussion

4.1 Control signals of a neuron and comparison of models

In natural situation of brain functioning, the membrane potential of a neuron is governed by external signals coming to the neuron, which are synaptic channel conductances. Therefore, any characteristics of neuronal activity must be measured as functions of the synaptic conductances. In assumption of their voltage independence, there are only two linear combinations of the synaptic conductances that control a neuron, and they can be chosen in the form of the total synaptic current measured at fixed voltage, u, and the total conductance s. Hence, the behavior of any neuronal model must be testified by changing u and s, at least. Unfortunately, not many models were compared with real neurons or to the HH model in this regard. Instead, alternative models are subject to tests with only current giving as an input. Here we impose the conditions of correct modelled responses to the both input signals. We focus on only steady-state spiking regime of neuronal activity, obtain experimental characteristics of this regime and compare models to experiments starting with the classical HH model.

4.2 Experimental 2d characteristics

In the paper, we have presented experimentally measured characteristics of a neuronal activity during prolonged stimulation. In order to avoid transient processes of adaptation, we excluded from the estimates the initial 500ms of the responses and took into account only the following 1s-lasting responses. With this clause, we consider the obtained characteristics as the ones for the steady state. As we have shown, the domain of the steady-state spiking is nontrivial in the planar space of the two input parameters, the input ("synaptic") current and conductance. Such domain has been previously visualized in the theoretical work with the HH model (Pokrovsky 1978) and in the experimental works (Chizhov et al. 2014; Smirnova et al. 2015), and it is consistent with the data presented as a series of f-I-curves in (Fernandez&White 2009, 2010; Fernandez et al. 2011; Graham & Schramm 2009). Such characteristics of the spiking regime as the spike threshold etc. have not been previously reported as functions of the two input parameters.

4.3 Advantages and disadvantages of the HH model

The HH model is a benchmark in mathematical neuroscience. It has been derived from the set of voltage-clamp experimental data that fully testifies possible behavior of ionic channels when the internal variable, the membrane potential is arbitrary changeable. In natural situation, as mentioned above, the membrane potential is governed by external signals coming to neuron, the synaptic channel conductances, and the effects of these signals can be mimicked by changing only u and s. The HH model which, by construction, combines the contributions of ionic currents, each being correctly governed by voltage, is expected to reproduce correctly the responses to arbitrary $u(t)$ and $s(t)$. Our comparison to experiments has confirmed this point for steady-state spiking regime. At least qualitatively, the model correctly reflects the shape of the domain of persistent spiking and the dependences of the firing rate on u and s, spike amplitude etc. However, quantitative agreement with data obtained from mammalian brain neuron has not been reached, even with the help of parameter fitting. We believe that this disagreement is based on contradictory requirements of high amplitude of spikes and low total conductance necessary for sensitivity to the external conductance s. In other words, the HH model qualitatively describes well the steady-state firing regime but quantitatively overestimates the conductances of voltage-gated channels.

4.3.1 Proposed model

A significant delay between a spike and the minimum of the membrane potential before the next spike is observed in a majority of experimental recordings in cortical and hippocampal pyramidal neurons (Amakhin et al. 2022; Ergina et al. 2021). The mechanisms underlying the delay are not fully understood. Hypothetically, this delay can be explained by either the delayed activation of hyperpolarizing currents like the potassium ones or by slow decay of depolarizing currents. The depolarizing currents are either membrane (presumably, sodium) currents or the currents

between neuronal branches. Although two-compartmental models (Pinsky and Rinzel 1994; Mainen and Sejnowski 1996) are able to reproduce this effect, in our work we could not find a set of parameters that would provide the match to all our requirements. This is the reason why, and also for the sake of simplicity, we supposed that this delay is caused by the relatively slow inactivation of sodium channels. Commonly, these channels are considered as persistent sodium channels comparatively to the fast-transient sodium channels. However, first, this consideration involves at least two activation variables for two types of channels. Second, the slowly inactivating channels are experimentally observed together with the fast channels, for instance, in pyramidal neurons of adult rats in contrary to their absence in new-born animals (Hamill et al. 1991). And third, the two currents differ in their kinetics because of different modes of gating rather than because of separate channel proteins (Alzheimer et al. 1993; Stafstrom 2007). For this reason, we approximate the sodium current as an exponentially closing one with a time constant of 7ms, thus cumulatively describing both transient and slow inactivating fractions of the channels, which provide voltage-clamp responses similar to that from (Hamill et al. 1991). Together with the slow potassium current, this current provides late voltage minimum and low firing rate. The fast potassium current shapes the repolarization phase of spikes. Its blockade in simulations affects similarly to the pharmacological blockade of fast potassium channels (Chen et al. 1996). Regarding DB, one can interprets this phenomenon in terms of the dynamic threshold, showing that the threshold “runs away” from the membrane potential, thus extending the dynamic threshold concept proposed in (Platkiewicz Brette 2010).

The shortcomings of the proposed model include too broad spikes and the lack of tendency to broaden spikes with the increasing stimulating current.

4.4 Depolarization block

As noted in (Bianchi et al. 2012), a model with only fast sodium and fast potassium currents is able to generate DB. With the help of a multicompartment model, the authors have found the necessary relations between the two currents, namely, relatively small window current for the sodium channels and relatively high-threshold of the potassium channel activation. At the same time, their single compartment model that matches experiments includes as many as ten currents, which points to the complexity of the problem. In (Tucker et al. 2012), it was found that DB results from the low density of somatic channels, and that low firing rate requires low window current. In contrast to that consideration, our explanation of DB mechanism is based on the threshold dynamics, i.e., the dependence of sodium channel activation on slow inactivation, where the slow inactivation is affected by the potassium channels. So, although DB is evident even in single compartment HH models because of the interaction between fast sodium and potassium channels, our modeling approach predicts that the DB effect at lower stimulating currents and conductances requires the dependence of sodium channel activation on inactivation, at least in single-compartment consideration. The importance of the slow inactivation of sodium channels

and the threshold dynamics for DB have been shown in (Qian et al. 2014). The authors notice that in the presence of slow inactivation, the effect occurs near or below the spike threshold, which ranges from -45 to -30mV in vitro. Otherwise, in the lack of slow inactivation, DB is qualitatively different, occurring at higher voltages and not possible in the experimentally observed range near -40mV. This study explains the difference in entering into DB, as suggested by (Bianchi et al. 2012) and our model.

4.5 Application of the proposed model for population model

Single-neuron models provide a base for mean-field models. An effective model of neuronal population has been proposed in (Chizhov and Graham 2007; Chizhov 2017), where such population was defined as a set of large number of similar neurons each receiving the same $u(t)$ and $s(t)$, and individual noise. The refractory density approach has been developed for the conductance-based neurons. One step of the method construction is the reduction of the full HH-like neuron to a threshold one. The proposed hybrid model is already a threshold-type model, so it can be implemented in the refractory density approach as an alternative to such basic neuron models as HH or integrate-and-fire ones. The implementation is straightforward. In this case, the advantages of the proposed model of a neuron are inherited by the population model, in particular, the reproduction of DB.

A. Appendix

A.1. Experimental technique

A.1.1. The whole-cell patch clamp recordings in rat brain slices

Animal handling and experimentation were performed in accordance with European Community Council directives 86/609/EEC. Male Wistar albino rats were used for the experiments (N=4, 18-21 days postnatal). Rats were sacrificed by decapitation, each brain was rapidly removed and immersed in ice-cold, preoxygenated (95 % O2 and 5 % CO2) artificial cerebrospinal fluid (ACSF) of the following composition (in mM): 126 NaCl, 2.5 KCl, 1.25 Na2HPO4, 24 NaHCO3, 2 CaCl2, 1 MgSO4, 10 D-glucose; pH 7.3-7.4. Coronal slices (300 μm thick) of medial frontal (prelimbic) cortex were cut with a vibratome (Microm HM 650 V; Microm, Walldorf, Germany). Slices were incubated at room temperature for at least 1 h before recordings. Neurons were visualized using transmitted illumination on a fixed-stage upright Axioscop 2 microscope (Zeiss, Oberkochen, Germany) equipped with differential interference contrast optics and a video camera (Grasshopper 3 GS3-U3-23S6M-C; FLIR Integrated Imaging Solutions Inc., Wilsonville, OR, USA). Pyramidal neurons were identified by their apical dendrites and triangular somata. Whole-cell recordings were made from layer 3 pyramidal neurons using Model 2400 (AM-Systems; Sequim, WA, USA) patch-clamp amplifier. Patch electrodes (3–5 MΩ) were pulled from borosilicate capillary glass (Sutter Instrument, Novato, CA, USA). The following internal solution

was used (in mM): 136 K-gluconate, 10 NaCl, 5 EGTA, 10 HEPES, 4 ATP-Mg, 0.3 GTP, pH 7.25 (adjusted with KOH).

A.1.2. Acquisition and dynamic-clamp

Signals were digitized with a sampling frequency of 33 kHz for acquisition with NI DAQ PCI-6221-37pin (National Instruments, Austin, TX) and filtered with 5KHz by the amplifier. Whole-cell recordings were done in the dynamic clamp mode to introduce additional leaky channel. The custom software ``DC-project" was used[1]. The applied current is calculated as $u(t) - s(t)(V(t) - V_{US})$, where $u(t)$ and $s(t)$ are the voltage-independent input signals, current and conductance, respectively; $V(t)$ is the membrane voltage and V_{US} is the reference voltage which was set to -60mV, close to the resting membrane potential V_{rest}. This reference voltage level is not essential, because its shift is equivalent to the shift of u. We included it for analysis only cells with stable input conductance and membrane potential, and with high access conductance. The access resistance was compensated in real time. For every neuron the recordings were started from estimations of the resting membrane potential V_{rest}, input conductance G_L, and the membrane time constant τ_m. Intrinsic membrane properties were assessed from the voltage responses to the series of 500-ms current steps providing hyperpolarization up to 5–10 mV.

To estimate the f-u-s-function in the whole domain of u and s that provide spike generation, a series of recordings were performed with the injected steps of input signal calculated for different values of current u and conductance s and lasting for 0.5 s with the frequency 0.5 Hz. The increments of u and s were constant, the typical grid was 25 by 12 for u and s, respectively. For each step of stimulation, the firing rate v was calculated as a total number of spikes per the last 2/3 of step duration. The values of u and s in the plots were scaled by the input conductance G_L, in order to compare Ω-domains for different neurons, following (Graham and Schramm, 2009).

The threshold was measured at the point where dV/dt reaches $5\,mV/ms$ or d^2V/dt^2 reaches $2\,mV/ms^2$. The spike half-width was measured for each spike at the half-height defined as the middle voltage level between the threshold and the peak, and averaged across all spikes of a trace. The post-spike hyperpolarization potential (PHP) was measured as a minimum value between spikes, and averages across spikes. The average membrane potential was calculated for each trace on interspike intervals since the time moment of the peak plus 2ms to the time of the next crossing of threshold.

A.2 Mathematical models

A.2.1 Hodgkin-Huxley model

We considered the classical one-compartmental Hodgkin-Huxley model, described by the following equations (Hodgkin and Huxley 1952):

[1] Available at: http://www.ioffe.ru/CompPhysLab/AntonV3.html

$$C\frac{dU}{dt} = -g_L(U - V_L) - \overline{g}_{Na}\, m^3\, h\, (U - V_{Na}) - \overline{g}_K\, n^4(U - V_K) + u(t) - s(t)(U - V_{us})$$

$$\frac{dm}{dt} = \frac{m_\infty - m}{\tau_m}, \quad \frac{dh}{dt} = \frac{h_\infty - h}{\tau_h}, \quad \frac{dn}{dt} = \frac{n_\infty - n}{\tau_n},$$

$$\tau_m = \frac{1}{\alpha_m + \beta_m}, \quad \tau_h = \frac{1}{\alpha_h + \beta_h}, \quad \tau_n = \frac{1}{\alpha_n + \beta_n},$$

$$m_\infty = \frac{\alpha_m}{\alpha_m + \beta_m}, \quad h_\infty = \frac{\alpha_h}{\alpha_h + \beta_h}, \quad n_\infty = \frac{\alpha_n}{\alpha_n + \beta_n},$$

$$\alpha_m = \frac{(U + 35)/10}{1 - \exp(-(U + 35)/10)}, \quad \beta_m = 4\exp\left(-\frac{U + 60}{18}\right),$$

$$\alpha_h = 0.07\exp\left(-\frac{U + 60}{20}\right), \quad \beta_m = \frac{1}{1 + \exp(-(U + 30)/10)},$$

$$\alpha_n = \frac{(U + 50)/100}{1 - \exp\,(-(U + 50)/10)}, \quad \beta_m = 0.125\exp\left(-\frac{U + 60}{80}\right)$$

where $U(t)$ is the membrane potential, C is the capacitance, V_L, V_{Na} and V_K are the leak, sodium and potassium reversal potentials, $m(U,t)$ is the sodium channel activation, $h(U,t)$ is the sodium channel activation, $n(U,t)$ is the potessium channel activation, g_L is the leak conductance, $\overline{g}_{Na}$ and $\overline{g}_K$ are the sodium and potassium channel maximum conductances.

$$C = 1\frac{\mu F}{cm^2}, \quad g_L = 0.3\frac{mS}{cm^2}, \; \overline{g}_{Na} = 120\frac{mS}{cm^2}, \quad \overline{g}_K = 36\frac{mS}{cm^2}$$

$$S = 1.4 \cdot 10^{-5} cm^2, \; (G_L = g_{tot}^0\, S = 5nS),$$

$$V_{rest} = -65\ mV, \; (V_L = -63\ mV), \; V_{us} = -60\ mV, \; V_K = -72\ mV, \; V_{Na} = 55\ mV$$

Here, in comparison with standard parameterization, the leak reversal potential V_L was modified to provide the desired resting potential V_{rest}, and the membrane area was set such that the input conductance at rest, G_L, would be equal to 5nS as in the other model.

A.2.2. Izhikevich model

The simple model of a regular spiking cell was used according to (Izhikevich, 2003), where to we introduced the input terms $u(t) - s(t)(U - V_{us})$:

$$C\,\frac{dU}{dt} = k(U - V_r)(U - V_t) - w + u(t) - s(t)(U - V_{us})$$

$$\frac{dw}{dt} = a\,(b\,(U - V_r) - w)$$

with the after-spike resetting

if $U \geq 30mV$, then $U = c$, $w = w + d$.

The parameters were normalized so that the neuron has an input conductance of 5nS, namely: $C = \left(100 * \frac{5}{35}\right) pF$, $k = \left(3 * \frac{5}{35}\right) nS/mV$, $V_r = -60\ mV$, $V_t = -50\ mV$, $a = \left(0.01 * \frac{35}{5}\right) ms^{-1}$, $b = \left(5 * \frac{5}{35}\right) nS$, $c = -60mV$, $d = 400\ pA$.

A.2.3. Minimal Hodgkin-Huxley-like model for rodent's cortical regular spiking neuron The model is taken from (Pospischil et al. 2008). A slow potassium channel with the activalion variable $p(U,t)$ was added to the original Hodgkin-Huxley model:

$$C\frac{dU}{dt} = -g_L(U - V_L) - \overline{g}_{Na}\, m^3\, h\, (U - V_{Na}) - \overline{g}_K\, n^4(U - V_K) - \overline{g}_M p(U - V_K) + u(t) - s(t)(U - V_{us})$$

$$\frac{dm}{dt} = \frac{m_\infty - m}{\tau_m}, \quad \frac{dh}{dt} = \frac{h_\infty - h}{\tau_h}, \quad \frac{dn}{dt} = \frac{n_\infty - n}{\tau_n}, \quad \frac{dp}{dt} = \frac{p_\infty - p}{\tau_p},$$

$$\tau_m = \frac{1}{\alpha_m + \beta_m}, \quad \tau_h = \frac{1}{\alpha_h + \beta_h}, \quad \tau_n = \frac{1}{\alpha_n + \beta_n},$$

$$m_\infty = \frac{\alpha_m}{\alpha_m + \beta_m}, \quad h_\infty = \frac{\alpha_h}{\alpha_h + \beta_h}, \quad n_\infty = \frac{\alpha_n}{\alpha_n + \beta_n},$$

$$\alpha_m = \frac{0.32(U - V_{Tr} - 13)}{1 - \exp(-(U - V_{Tr} - 13)/4)}, \quad \beta_m = \frac{-0.28(U - V_{Tr} - 40)}{1 - \exp(-(U - V_{Tr} - 40)/5)},$$

$$\alpha_h = 0.128 \exp\left(-\frac{U - V_{Tr} - 17}{18}\right), \quad \beta_m = \frac{4}{1 + \exp(-(U - V_{Tr} - 40)/5)},$$

$$\alpha_n = \frac{0.032(U - V_{Tr} - 15)}{1 - \exp\left(-(U - V_{Tr} - 15)/5\right)}, \quad \beta_m = 0.5 \exp\left(-\frac{U - V_{Tr} - 10}{40}\right),$$

$$p_\infty = \frac{1}{1 + \exp(-(U + 35)/10)}, \quad \tau_p = \frac{\tau_{max}}{3.3\ \exp((U + 35)/20) + \exp(-(U + 35)/20)},$$

$C = 1\frac{\mu F}{cm^2}$, $g_L = 0.1\frac{mS}{cm^2}$, $\overline{g}_{Na} = 50\frac{mS}{cm^2}$, $\overline{g}_K = 5\frac{mS}{cm^2}$, $\overline{g}_M = 0.07\frac{mS}{cm^2}$, $S = 29 \cdot 10^{-5} cm^2$, $V_L = -70\ mV$, $V_{us} = -60\ mV$, $V_K = -90\ mV$, $V_{Na} = 50\ mV$, $V_{Tr} = -60\ mV$, $\tau_{max} = 1\ s$.

A.2.4. The proposed hybrid model

The proposed model contains three channels: one sodium channel I_{Na} and two potassium channels, one fast $I_{K,f}$ and one slow $I_{K,s}$. The voltage equation hence reads:

$$C\frac{dU}{dt} = -g_L(U - V_L) - I_{Na} - I_{K,f} - I_{K,s} + u(t) - s(t)(U - V_{us}) \quad (1)$$

The sodium current is defined by:

$$I_{Na}(U,t) = \overline{g}_{Na}\, m^2(U,t)\, i(U,t)\, (U(t) - V_{Na}), \tag{2}$$

$$\text{if} \quad \big(U(t) > V^T(t)\big)\, and\, (h > 0.5) \quad \text{then} \quad m = 1,\, h = 0 \tag{3}$$

$$V^T(t) = -51 + ((i_\infty^{-1}(i(t)) + 60)/5)^2\, mV \tag{4}$$

$$\frac{dm}{dt} = \frac{m_\infty - m}{\tau_{mm}} \tag{5}$$

$$\frac{dh}{dt} = \frac{i_\infty - h}{\tau_h} \tag{6}$$

$$\frac{di}{dt} = \frac{i_\infty(U) - i}{\tau_i(U)} \tag{7}$$

$$\tau_{mm} = 7\, ms,\ \tau_h = 10ms,\ \tau_i = 40\, ms,\ m_\infty = 0,$$

$$i_\infty = 1/(1 + exp(\,(U + 44)/4)), \quad \text{hence}\ \ i_\infty^{-1}(x) = -44 + 4\ln(1/x - 1)$$

The fast voltage-dependent potassium current $I_{K,f}$ is defined by:

$$I_{K,f}(U,t) = \overline{g}_{K,f}\, n(U,t)(U(t) - V_K), \tag{8}$$

$$\frac{dn}{dt} = \frac{n_\infty(U) - n}{\tau_n(U)}, \tag{9}$$

$$\tau_n = 1/(a+b) + 2\, ms;\ \ n_\infty = a/(a+b),$$

$$a = 0.1\, exp(\,(U + 25)/7)\, ms^{-1},\ b = 0.1\, exp(-(U + 25)/7)\, ms^{-1}$$

The slow voltage-dependent potassium current $I_{K,s}$ is defined by:

$$I_{K,s}(U,t) = \overline{g}_{K,s}\, w(U,t)\ \ (U(t) - V_K), \tag{10}$$

$$\frac{dw}{dt} = \frac{w_\infty(U) - w}{\tau_w(U)}, \tag{11}$$

$$\tau_w = 1/(a+b) + 4\, ms,\ \ w_\infty = a/(a+b),$$

$$a = 5\exp(U/4)\, ms^{-1},\ b = 0.05\, ms^{-1}$$

Parameters values are given by:

$$C = 0.7\, \mu F/cm^2,\ \ \tau_m = C/g_{tot}^0 = 14.4\, ms,\ \ (g_L = 0.048\, \mu S/cm^2),$$

$$S = 10^{-4}\, cm^2,\ (G_L = g_{tot}^0\, S = 5nS),$$

$$V_{rest} = -65\ mV,\ (V_L = -65\ mV),\ \ V_{us} = -60\ mV,\ V_K = -80\ mV,\ V_{Na} = 55\ mV,$$

$$\overline{g}_{Na} = 2\,\frac{\mu S}{cm^2}, \quad \overline{g}_{K,f} = 2\,\frac{\mu S}{cm^2}, \quad \overline{g}_{K,s} = 0.5\,\frac{\mu S}{cm^2}.$$

For a fast-spiking interneuron, not considered in the present paper, we modified two parameters: $\overline{g}_{K,s} = 0.1\,\frac{\mu S}{cm^2}$ and $\tau_{mm} = 3\,ms$, which increases the gain of the f-I curve, increases the maximum firing rate and approaches the DB limit.

A.2.5. The proposed continuous model

A continuous version of the sodium channel approximation is obtained from the system of eqs.(1-11) by omitting the threshold condition, eq.(3), and introducing in eqs.(5,6) the variable time constants and steady-state functions in the following form:

$$\tau_{mm} = 0.1\,ms + 7ms\,(1 - S_V S_h),$$

$$\tau_h = 0.1\,ms + 10ms\,(1 - S_V S_m),$$

$$m_\infty = S_V S_h,$$

$$h_\infty = (1 - S_V S_m)\,i_\infty(U(t)),$$

$$S_V = 1/\big(1 + \exp\big(-\big(U(t) - V^T(t)\big)/0.1mV\big)\big),$$

$$S_h = 1/(1 + \exp(-(h(t) - 0.5)/0.01)),$$

$$S_m = 1/(1 + \exp(-(m(t) - 0.8)/0.01)).$$

A.2.6 Statistical analysis

For each spike, the threshold potential in the model was measured at 1.2ms before the peak of the spike. The spike half-width was measured for each spike at the voltage level -20mV, and averaged across all spikes of a trace. The post-spike hyperpolarization potential (PHP) was measured as a minimum value between spikes, and averages across spikes. The average membrane potential was calculated for each trace on interspike intervals since the time moment of the peak plus 2ms to the point where dV/dt reaches $5\,mV/ms$.

Funding

This work was supported by the Russian Science Foundation (project 21-15-00416) for D.A.

References

Alzheimer C, Schwindt PC, Crill WE (1993) Modal gating of Na^+ channels as a mechanism of persistent Na^+ current in pyramidal neurons from rat and cat sensorimotor cortex. J Neurosci. 13:660–673.

Amakhin DV, Soboleva EB, Postnikova TYu, Tumanova NL, Dubrovskaya NM, Kalinina DS, Vasiliev DS, Zaitsev AV (2022) Maternal Hypoxia Increases the Excitability of Neurons in the Entorhinal Cortex and Dorsal Hippocampus of Rat Offspring // Frontiers in Neuroscience 16:867120. DOI: 10.3389/fnins.2022.867120.

Berndt A, Lee SY, Ramakrishnan C, Deisseroth K (2014) Structure-Guided Transformation of Channelrhodopsin into a Light-Activated Chloride Channel. Science 344:420-424.Bianchi D, Marasco A, Limongiello A, Marchetti C, Marie H, Tirozzi B, Migliore MJ (2012) On the mechanisms underlying the depolarization block in the spiking dynamics of CA1 pyramidal neurons. Comput Neurosci 33(2):207-225.

Borg-Graham LJ, Monier C, Fregnac Y (2003) Visual input evokes transient and strong shunting inhibition in visual cortical neurons. Nature 393(6683):369-373.

Brette R, Gerstner W (2005) Adaptive exponential integrate-and-firemodel as an effective description of neuronal activity. J Neurophysiol 94(5):3637-3642.

Chen W, Zhang JJ, Hu GY, Wu CP (1996) Different mechanisms underlying the repolarization of narrow and wide action potentials in pyramidal cells and interneurons of cat motor cortex. Neuroscience 73(1):57-68.

Chizhov AV (2017) Conductance-Based Refractory Density Approach: Comparison with Experimental Data and Generalization to Lognormal Distribution of Input Current. Biol Cybernetics 111(5-6):353-364.

Chizhov AV, Amakhin DV, Zaitsev AV. (2019) Mathematical model of Na-K-Cl homeostasis in ictal and interictal discharges. PLoS One 14(3):e0213904.

Chizhov AV, Graham LJ (2007) Population model of hippocampal pyramidal neurons, linking a refractory density approach to conductance-based neurons. Phys Rev E 75:011924.

Chizhov AV, Smirnova E Yu, Kim K Kh, Zaitsev AV (2014) A simple Markov model of sodium channels with a dynamic threshold. J Comp Neuroscience 37(1):181-191, 2014.

Cressman JR, Ullah G, Ziburkus J, Schiff SJ, Barreto E (2009) The influence of sodium and potassium dynamics on excitability, seizures, and the stability of persistent states: I. Single neuron dynamics. J Comput Neurosci 26(2):159–170.

Destexhe A, Bal T (2009) Dynamic clamp: from principles to applications. Springer.

Dovzhenok A, Kuznetsov AS (2012) Exploring neuronal bistability at the depolarization block. PLoS ONE 7(8):e42811.

Ergina JL, Amakhin DV, Postnikova TY, Soboleva EB, Zaitsev AV (2021) Short-term epileptiform activity potentiates excitatory synapses but does not affect intrinsic membrane properties of pyramidal neurons in the rat hippocampus in vitro. Biomedicines 10(9):1374.

Fernandez, FR, Broicher T, Truong A, White JA. Membrane voltage fluctuations reduce spike frequency adaptation and preserve output gain in CA1 pyramidal neurons in a high conductance state. Journal of Neuroscience, 31(10), 3880–3893, 2011.

Fernandez FR, White JA (2009) Reduction of spike after depolarization by increased leak conductance alters interspike interval variability. J Neurosc 29(4):973–986

Fernandez FR, White JA (2010) Gain control in CA1 pyramidal cells using changes in somatic conductance. J Neurosc 30(1):230–241.

Gerstner W, Naud R (2009) How Good Are Neuron Models? Science 326(5951):379-380.

Górski T, Depannemaecker D, Destexhe A (2021) Conductance-Based Adaptive Exponential Integrate-and-Fire Model. Neural Computation 33:41-66.

Graham LJ, Schramm A (2009) In vivo dynamic clamp: The functional impact of synaptic and intrinsic conductances in visual cortex. In A. Destexhe, & T. Bal (Eds.), Dynamic clamp: From principles to applications. Springer Press, 2009.

Gutkin B, Ermentrout GB (2006) Spikes too kinky in the cortex? Nature 440(7087):999–1000.

Hamill OP, Huguenard JR, Prince DA (1991) Patch-clamp studies of voltage-gated currents in identified neurons of the rat cerebral cortex. Cerebral Cortex 1:48-61.

Hodgkin AL, Huxley AF (1952) A quantitative description of membrane current and its application to conduction and excitation in nerve. J Physiol 117(4):500–544.

Izhikevich EM (2003) Simple model of spiking neurons. IEEE Transactions on Neural Networks 14:1569-1572.

Krishnan GP, Bazhenov M (2011) Ionic dynamics mediate spontaneous termination of seizures and postictal depression state. J Neurosci 31(24):8870–8882.

Mainen ZF, Sejnowski TJ (1996) Influence of dendritic structure on firing pattern in model neocortical neurons. Nature 382, 363–366.

McCormick DA, Shu Y, Yu Y (2007) Neurophysiology: Hodgkin and Huxley model–still standing? Nature 445:E1–2.Naundorf B, Wolf F, Volgushev M (2006) Unique features of action potential initiation in cortical neurons. Nature 440(7087):1060–1063.

Pinsky PF, Rinzel J (1994) Intrinsic and network rhythmogenesis in a reduced Traub model for CA3 neurons. J Comput Neurosci 1(1-2):39–60.

Platkiewicz J, Brette R (2010) A Threshold Equation for Action Potential Initiation. PLoS Comput Biol 6(7): e1000850.

Pokrovskii AN (1978) Effect of synapse conductivity on spike development. Biofizika 23(4):649–653.

Pospischil M, Monier C, Piwkowska Z, Bal T, Frégnac Y, Destexhe A (2008) Minimal Hodgkin–Huxley type models for different classes of cortical and thalamic neurons. Biol Cybern 99:427–441.

Prinz AA, Abbott LF, Marder E (2004) The dynamic clamp comes of age. Trends Neurosci 27:218-224.

Qian K, Yu N, Tucker KR, Levitan ES, Canavier CC (2014) Mathematical analysis of depolarization block mediated by slow inactivation of fast sodium channels in midbrain dopamine neurons. J Neurophysiol 112(11):2779-90.

Rinzel J, Baer SM (1988) Threshold for repetitive activity for a slow stimulus ramp: a memory effect and its dependence on fluctuations. Biophys J 54(3):551-555.

Schwalger T, Chizhov A (2019) Mind the Last Spike -- Firing Rate Models for Mesoscopic Populations of Spiking Neurons. Curr Opinion in Neurobiology 58:155-166.

Shao L-R, Halvorsrud R, Borg-Graham L, Storm JF (1999) The role of BK-type Ca-dependent K-channels in spike broadening during repetitive firing in rat hippocampal pyramidal cells. J Physiol 521(1):135-146.

Shriki O, Hansel D, Sompolinsky H (2003) Rate models for conductance-based cortical neuronal networks. Neural Comput 15(8):1809-41.

Smirnova EY, Zaitsev AV, Kim KKh, Chizhov AV (2015) The domain of neuronal firing on a plane of input current and conductance. J Comput Neurosci. 39(2):217-33.

Stafstrom CE (2007) Persistent sodium current and its role in epilepsy. Epilepsy Curr 7(1):15-22. Tucker KR, Huertas MA, Horn JP, Canavier CC, Levitan ES (2012) Pacemaker rate and depolarization block in nigral dopamine neurons: a somatic sodium channel balancing act. J Neurosci 32(42):14519-31.

Vervaeke K, Hu H, Graham LJ, Storm JF (2006) Contrasting Effects of the Persistent Na+ Current on Neuronal Excitability and Spike Timing. Neuron 49:257–270.

Wei Y, Ullah G, Ingram J, Schiff SJ (2014) Oxygen and seizure dynamics: II. Computational modeling. J Neurophysiol 112:213–223.